Front. Earth Sci.
https://doi.org/10.1007/s11707-024-1100-7

RESEARCH ARTICLE

A new parameter for characterizing pore-fracture structure heterogeneity: fractal dimension based on the mercury extrusion curve

Junjian ZHANG[1], Anan XU[2], Chengjin ZHAO (✉)[3,4], Wei WANG[5], Youlu JIANG (✉)[4], Veerle VANDEGINSTE[6], Zhengbao XUE[7], Yuqiang GUO[1], Heyao MIAO[2]

1 College of Earth Sciences & Engineering, Shandong University of Science and Technology, Qingdao 266590, China
2 School of Management, Changchun University, Changchun 130000, China
3 Geosteering & Logging Research Institute, Sinopec Matrix Corporation, Qingdao 266000, China
4 School of Geosciences, China University of Petroleum (East China), Qingdao 266580, China
5 Exploration and Development Research Institute of PetroChina Southwest Oil & Gas Field Company, Chengdu 610041, China
6 Department of Materials Engineering, KU Leuven, Bruges, 8200 Bruges, Belgium
7 The Second Exploration Team of Shandong Coalfield Geology Bureau, Jining 272000, China

Abstract Pressure mercury intrusion test is (MIP) one of the most commonly used methods to characterize pore-fracture structure. Here, we use the fractal dimension of the mercury intrusion curve to analyze the heterogeneity of pore and fracture distribution. Differing from the intrusive mercury curve, the extrusive curve provides a better representation of the seepage capacity of a reservoir. In this paper, the division method of sample types using both mercury invasive parameters (pore volume, pore volume percentage, porosity, permeability) and extrusive parameters (mercury removal efficiency) is discussed. The fractal dimension values of mercury intrusive and extrusive curves are calculated for all samples using the Menger, Thermodynamics, and Multifractal fractal models. Moreover, the fractal significance of the mercury withdrawal curve is examined. The results are as follows. 1) The samples can be divided into three types based on the mercury removal efficiency and total pore volume. Type A is characterized by lower total pore volume (< 0.08 $cm^3 \cdot g^{-1}$) and removal efficiency (< 30%), type B has lower total pore volume (< 0.08 $cm^3 \cdot g^{-1}$) and higher removal efficiency (> 30%), and type C has larger total pore volume (> 0.08 $cm^3 \cdot g^{-1}$) and higher removal efficiency(> 30%). 2) Mercury removal efficiency does not correlate with the mineral composition or total pore volume, but it does show a clear positive correlation with pore volume in the range of 100 to 1000 nm. Unlike the Menger model, the mercury removal curve analyzed using the thermodynamics and multifractal model shows good fractal characteristics. 3) In contrast to the injective curves, the fractal dimension of mercury removal curves exhibits an obvious linear negative correlation with pore structure parameters and mercury removal efficiency. Moreover, the multifractal dimensions D_0–D_{10} obtained from the mercury removal curves show a negative correlation with porosity and permeability. This indicates that fractal dimension based on the mercury extrusion curve can be used as a new parameter for characterizing pore-fracture structure heterogeneity.

Keywords pore-fracture structure, mercury extrusion curve, pore structure, porosity, permeability

1 Introduction

The pores and fracture structures in tight sandstone play a crucial role in restricting oil-water-gas seepage and production. Various technologies, such as high pressure mercury injection experiments (HPMI), low-temperature nitrogen and carbon dioxide gas adsorption (LPN_2/CO_2 GA), and low field nuclear magnetic resonance (LF-NMR), are currently used to characterize unconventional reservoirs (Lai et al., 2018; Su et al., 2018; Hou et al., 2020, 2023; Zhang et al., 2020; Wang et al., 2023). Given the range in pore sizes in tight sandstone, different methods are selected accordingly.

In contrast to other testing methods, HPMI provides a

Received February 8, 2023; accepted July 21, 2023

E-mails: zhaochengjint_t@163.com (Chengjin ZHAO)
jiangyoulu@upc.edu.cn (Youlu JIANG)

quantitative characterization of the nano-micro-pore structure by measuring the mercury injection volume under different injection pressures. Parameters such as pore volume and specific surface area are then calculated (Schmitt et al., 2013; Guo et al., 2014; Peng et al., 2017; Zhang et al., 2022c). Because of its advantage of being faster, simpler, and more cost-effective, it has become one of most commonly used methods for characterizing the structure of unconventional reservoirs. At present, extensive literature examines the shape of the mercury injection curve and injective volume, pore types, pore size distribution, and the dynamic variation of porosity-permeability influenced by this curve. However, research on the mercury removal curve remains relatively scarce, with only the mercury removal efficiency being investigated (Zhang et al., 2022c). Compared with the mercury injection curve, it has been established that the mercury withdrawal curve is better suited to characterize the migration of gas and water (Cai et al., 2018). Therefore, further research on mercury removal curves is needed.

Since quantitative analysis of pore-fracture systems using traditional geometric methods is challenging, fractal theory based on HPMI tests has emerged as the preferred approach for quantitative characterization of pore structure heterogeneity (Knackstedt et al., 1996; Cai et al., 2016, 2018; Su et al., 2018; Li et al., 2020). Typical fractal models include Menger, Thermodynamic fractal (Zhang et al., 2006), and Multifractal models (Song et al., 2018). The mentioned fractal models rely on mercury injection curves as data sources, and fractal dimension is calculated to examine the pore-fracture structure heterogeneity of the reservoir itself. However, the fractal nature of the mercury removal curve and its impact on changes in porosity and permeability remains to be investigated.

In this study, 20 sandstone samples from the Xujiahe Formation were selected from wells in the Sichuan Basin (Fig. 1). The method to classify sample types using both mercury intrusion parameters (pore volume, pore volume percentage, porosity, permeability) and extrusive parameters (mercury removal efficiency) is discussed. The fractal dimension values of the mercury injection and removal curves are calculated for all samples using the Menger, Thermodynamics and Multifractal fractal models. Moreover, the fractal significance of the mercury withdrawal curve is explored. Finally, the relationship between the fractal dimension values obtained from the mercury removal curve and porosity-permeability is examined.

2 Geological setting of sampling site

The Sichuan Basin is a superimposed basin, developed on the upper Yangtze Craton, located in south-west China (He et al., 2011). The study area is located north-east of Sichuan Basin (Fig. 1(a)), structurally bounded by the Longmen mountain thrust belt to the west, the Micang mountain orogenic belt to the north, and the Daba mountain thrust nappe belt to the east. It has undergone multiple tectonic movements since the Triassic, including the Indosinian, Yanshanian, and Himalayan structural movements, and can be divided into five substructural units. Previous studies have indicated that the provenance of the Xujiahe Formation is from the three peripheral orogenic belts and that the formation has characteristics of a multi-source mixture (Fig. 1(b)). The Xujiahe Formation (T_3x) consists of coal-bearing strata developed in a lake delta environment (Fig. 1(b)). Its main facies include underwater distributary channels, braided river delta plains, shore-shallow lacustrine facies, distributary bays, peat swamp facies and others. The total strata thickness of the T_3x strata ranges from 270 to 730 m, and can be divided into five members sections, i.e., from T_3x^1 to T_3x^5 (Zhang et al., 2009; Wang et al., 2023). A 1D basin model shows that the Xujiahe Formation has experienced a maximum burial depth 5600−6800 m and reached a maximum paleotemperature of 180°C−220°C. It has undergone almost 100 Ma tectonic uplift with a total exhumation of 1200−2800 m (Zhao et al., 2022).

Twenty fresh shale samples (approximately 15 × 15 × 15 cm^3) were collected from a single well, and their distribution and parameters are shown in Fig. 1 and Table 1. Gas porosity (%) and permeability (mD) of the core samples were measured using an Ultrapore-200A helium core porosimeter and CMS-300 Automated Permeameter. The mineral composition of each sample was analyzed, and the pore volume, specific surface area and pore size distribution were quantitatively studied using HPMI tests. The analysis scheme is as follows. HPMI analysis was conducted on the samples using an IV9500 mercury intrusion instrument. One hundred 20 pressure points were measured for each sample with an analysis time of 5 s for each end. The working pressure of the mercury intrusion analyses ranged from 0.124 to 270.79 MPa.

The following section discusses three fractal models, with detailed process information can be found in Zhang et al. (2022a, 2022b).

Menger fractal model:

$$\lg(\mathrm{d}V_{\mathrm{obs}}/\mathrm{d}P) \infty (D-4)\lg P, \tag{1}$$

where D represents the value of a fractal dimension, dimensionless; P represents the injection pressure, MPa; V represents injection volume of mercury, $cm^3 \cdot g^{-1}$;

Thermodynamic fractal model:

$$\mathrm{d}W = -P\mathrm{d}v = -r_{\mathrm{L}}\cos\theta \mathrm{d}S, \tag{2}$$

where v is pore volume, $cm^3 \cdot g^{-1}$; W is the surface energy; r_{L} is the surface tension between mercury and surface, J/m; θ is the contact angle between mercury and pore

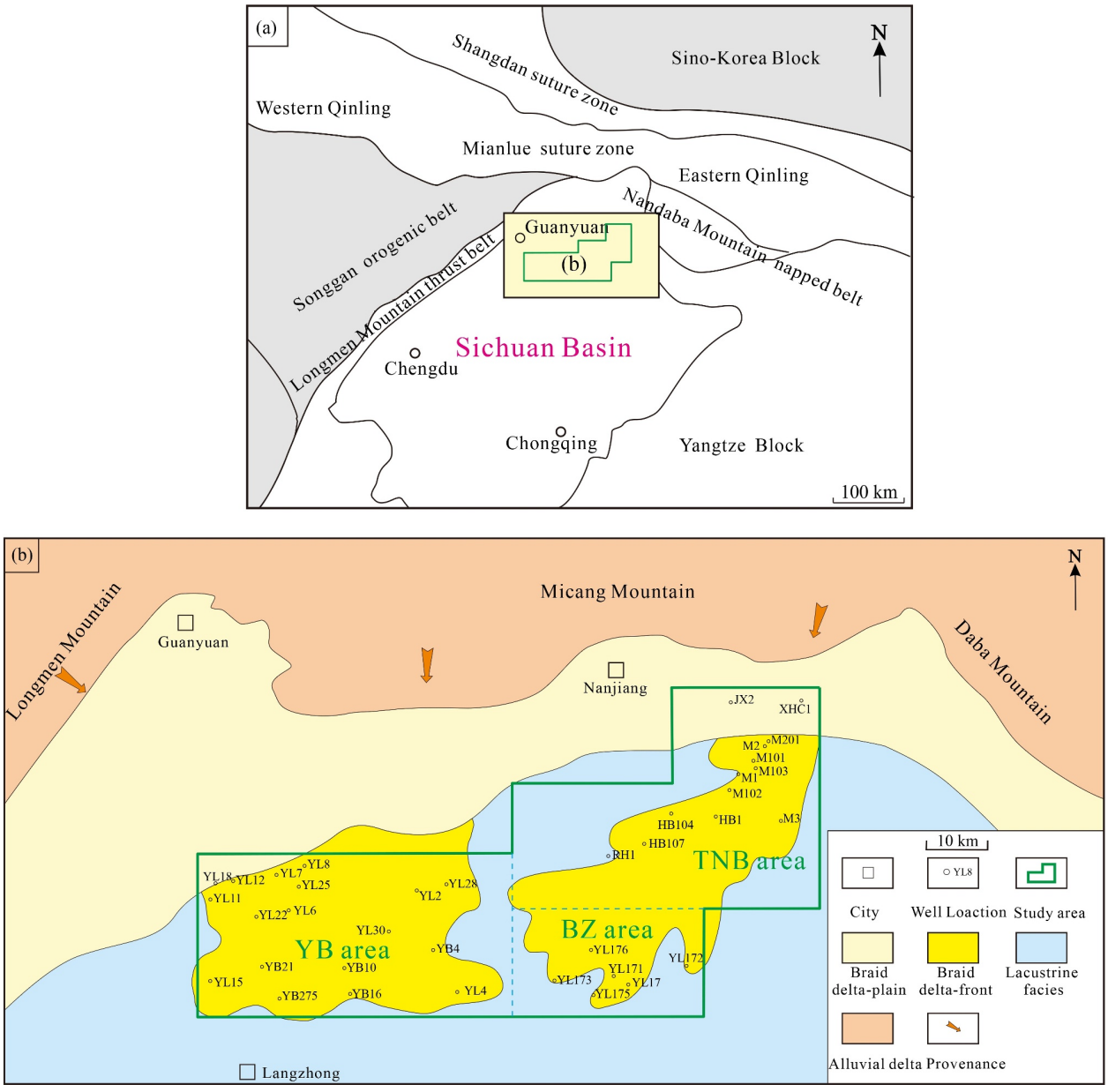

Fig. 1 (a) Structural sketch of Sichuan Basin and location of the study area; (b) Well location distribution and sedimentary environment of the study area (modified from Zhao et al., 2022). YB area = Yuanba area; BZ area = Bazhong area; TNB area = Tongnanba area.

surface (approximately 140°); and S is the specific pore surface, $m^2 \cdot g^{-1}$

Multi-fractal model. *a–f* (a) is a set of primary languages describing the local features of multifractals, called multifractal spectrum. Another set *q–D* (q) is introduced from the information theory perspective and is known as the generalized fractal dimension. A detailed description is available in previous studies (Hu et al., 2020; Zhang et al., 2022a, 2022b).

Generalized fractal dimension are selected as an example, parameter D_q includes D_{-10}, D_{10}, D_{-10}–D_{10}, D_0–D_{10}, and D_{-10}–D_0. D_q is a monotonically decreasing function with a sigmoidal shape. D_{-10} is influenced by the lowest probability measure areas, whereas D_{10} is effected by highest probability measure areas. D_0–D_{10} and D_{-10}–D_0 are the amplitudes of the right and left branches of D_q, which represents the high and low probability measure areas heterogeneity, respectively (Zhang et al., 2020).

The data sources of the mentioned fractal models are all mercury injection curves, and the fractal dimension is calculated to analyze the heterogeneity of the pore-fracture structure in the reservoir. It is important to investigate whether the mercury removal curve exhibits fractal characteristics, and its impact on changes in porosity and permeability. The fractal dimensions of the three fractal models were calculated based on the mercury removal

curve of the same set of samples. The differences in fractal characteristics between the mercury injection curve and withdrawal curve of these samples are discussed.

3 Results

3.1 Sample type classification and pore-fracture system of all samples

The mineralogical composition of all sandstone samples is presented in Table 1. The clay content ranges from 1% to 11%, whereas the quartz content varies from 10% to 94%, and the feldspar content ranges from 0 to 18%. These results indicate that the samples are primarily composed of quartz, which is favorable for reservoir reconstruction. The porosity-permeability results show that the porosity of the samples ranges from 0.50% to 4.22%, whereas the permeability varies from 0.002 to 5.42 mD. Except for sample 9, most of the samples have low porosity and low permeability. Based on differences in research objectives, literature classifies the sample types according to factors such as pore structure parameters and mineral components. Figure 2 shows four types of sample classification schemes based on pore structure parameters (total pore volume, pore volume percentage of 10−100 nm and < 100 nm), porosity and mercury removal efficiency. Since this study focuses on the mercury removal curve, the mercury removal efficiency and total pore volume are selected to classify the samples into three categories.

Figure 3(a) shows that the mercury injection curve of type A samples remains nearly horizontal when the mercury pressure is less than 100 MPa, indicating a lack of developed pore-fracture structure. The mercury removal curve for type A samples is almost flat, suggesting a complex pore structure with minimal mercury removal. Type B samples exhibit a nearly horizontal mercury injection curve at pressures below 1 MPa, indicating the absence of larger pores. However, the mercury injection curve becomes nearly vertical for the pressure range of 1 to 100 MPa, indicating the presence of smaller pores. The mercury removal curve for type B samples is almost vertical, suggesting a more straightforward pore structure with a larger amount of mercury removal (Fig. 3(b)). Type C samples display intermediate characteristics between type A and type B, representing a transitional type.

The pore volume of type B samples is greater than that of types A and C, which is consistent with the results in Fig. 3. Moreover, the mercury removal efficiency of type B samples is larger than that of types A and C. This

Table 1 Basic information of all samples

Sample No.	Porosity/%	Permeability/mD	Mineral composition/%			
			Clay content	Quartz	Feldspar	Carbonate minerals
1	0.34	0.002	4	42	4	49
2	3.47	0.003				
3	1.45	0.1542				
4	1.28	0.0676	6	75	14	5
5	2.03	0.003				
6	3.97	0.0334				
7	1.12	0.0028	1	10	0	89
8	2.04	0.006	1	16	0	83
9	1.33	5.412	1	14	0	85
10	1.42	0.002	11	70	13	6
11	1.42	0.003				
12	6.81	0.035	5	76	16	2
13	4.51	0.012	6	73	18	3
14	2.79	0.0032	7	74	16	2
15	2.51	0.003	3	22	0	75
16	4.22	0.009				
17	1.17	0.0015	1	17	0	82
18	0.50	0.0026				
19	4.06	0.0306	3	94	0	2
20	7.48	0.0261	5	74	12	5

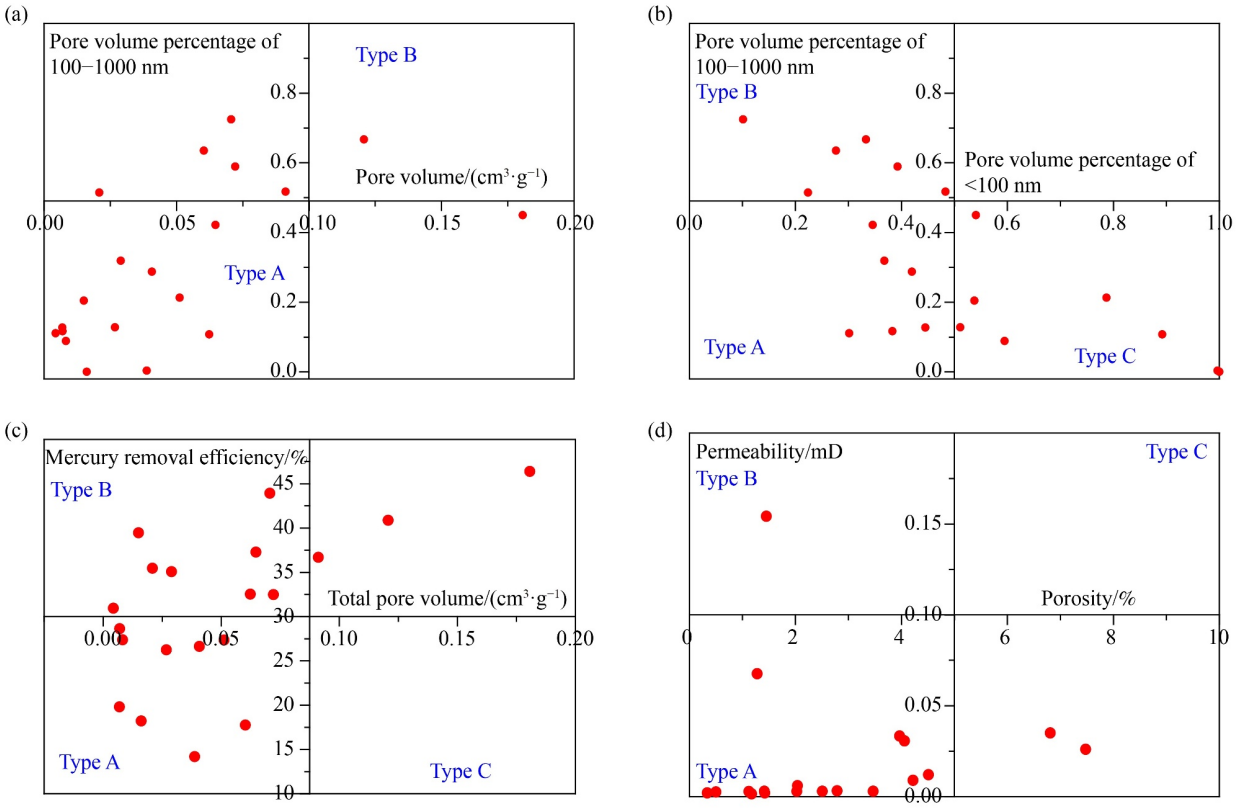

Fig. 2 Sample classification results based on high pressure mercury injection test parameters.

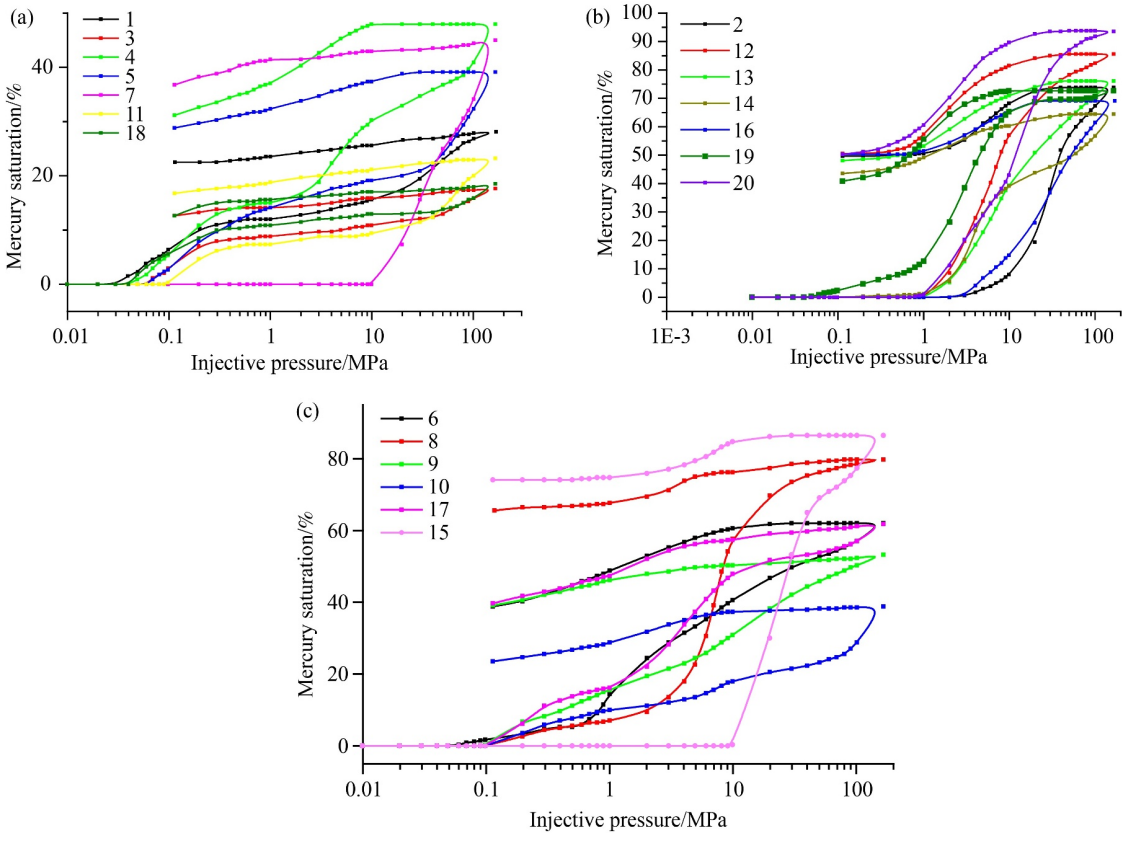

Fig. 3 Mercury injection and withdrawal curves of different sample types.

indicates that type B samples have a larger pore volume, higher mercury removal efficiency, and a more favorable pore structure, making them the focus of further research (Figs. 4(a) and 4(b)). Compared with Fig. 4(c), the pore volume percentage of micro-pores (pore diameter less than 100 nm) of all samples ranges from 0.2 to 0.8, with minimal variation among different types. The meso-pore (100−1000 nm) volume percentage of type B and C samples is higher than that of type A samples, and the macro-pore (more than 1000 nm) volume percentage of type A and C samples is higher than that of type B samples (Fig. 4(c)).

3.2 Fractal characteristics using the thermodynamic model

The results of the thermodynamic fractal dimension, based on Eq. (2) and the mercury injection and withdrawal curves are shown in Fig. 5. Figures 5(a), 5(b), and 5(c) indicate that mercury removal curve still exhibits fractal characteristics when using a thermodynamic model. However, the fractal dimension obtained from the mercury injection curve is higher than that of mercury withdrawal curve. Figure 5(d) shows no apparent correlation between the fractal dimension obtained from the mercury injection curve and the fractal dimension obtained from the mercury withdrawal curve. Moreover, Figure 5(e) suggests that the difference in fractal dimension obtained from the mercury injection curve among different sample types is relatively minor. However, Figure 5(f) shows that the fractal dimension obtained from the mercury withdrawal curve for type B samples is smaller than that for type A and C samples, indicating that the fractal dimension obtained from the mercury withdrawal curve better reflects the differences among these samples.

3.3 Fractal characteristics using the multi-fractal model

The results of the multi-fractal dimension, using the mercury injection and withdrawal curves, are shown in Fig. 6. Figures 6(a), 6(b), and 6(c) indicate that the mercury removal curve still exhibits fractal characteristics when using the multi-fractal model. Moreover, D_{-10}–D_0 obtained from the mercury injection curve is larger than that obtained from the mercury withdrawal curve, and D_0–D_{10} obtained from the mercury injection curve is smaller than that obtained from the mercury withdrawal curve. Moreover, within a single sample, the D_{-10}–D_0 value is larger than the D_0–D_{10} value. Figures 6(d), 6(e), and 6(f) indicate no apparent correlation between the fractal dimension obtained from the mercury injection curve and the fractal dimension obtained from the mercury withdrawal curve.

Figure 7(a) shows that the difference in fractal dimension obtained from the mercury injection curve among different sample types is relatively smaller. However,

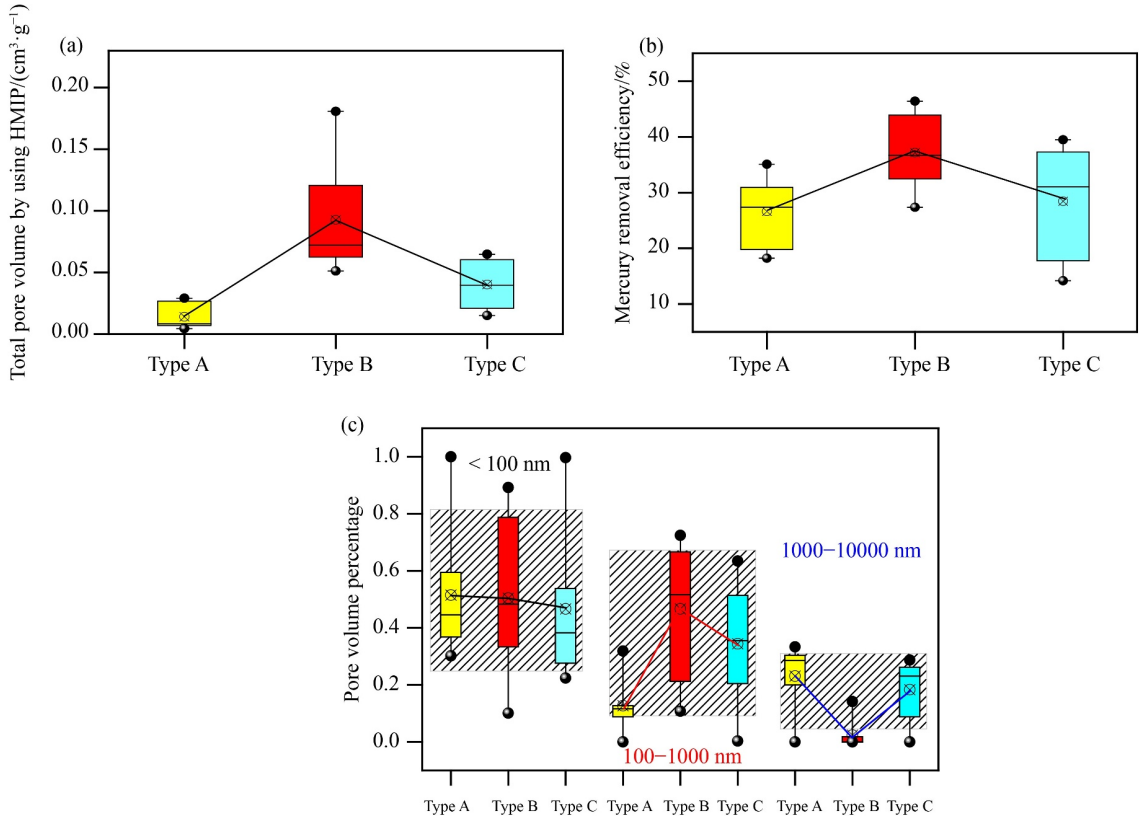

Fig. 4 Comparison of the pore volume and mercury removal efficiency in different sample types.

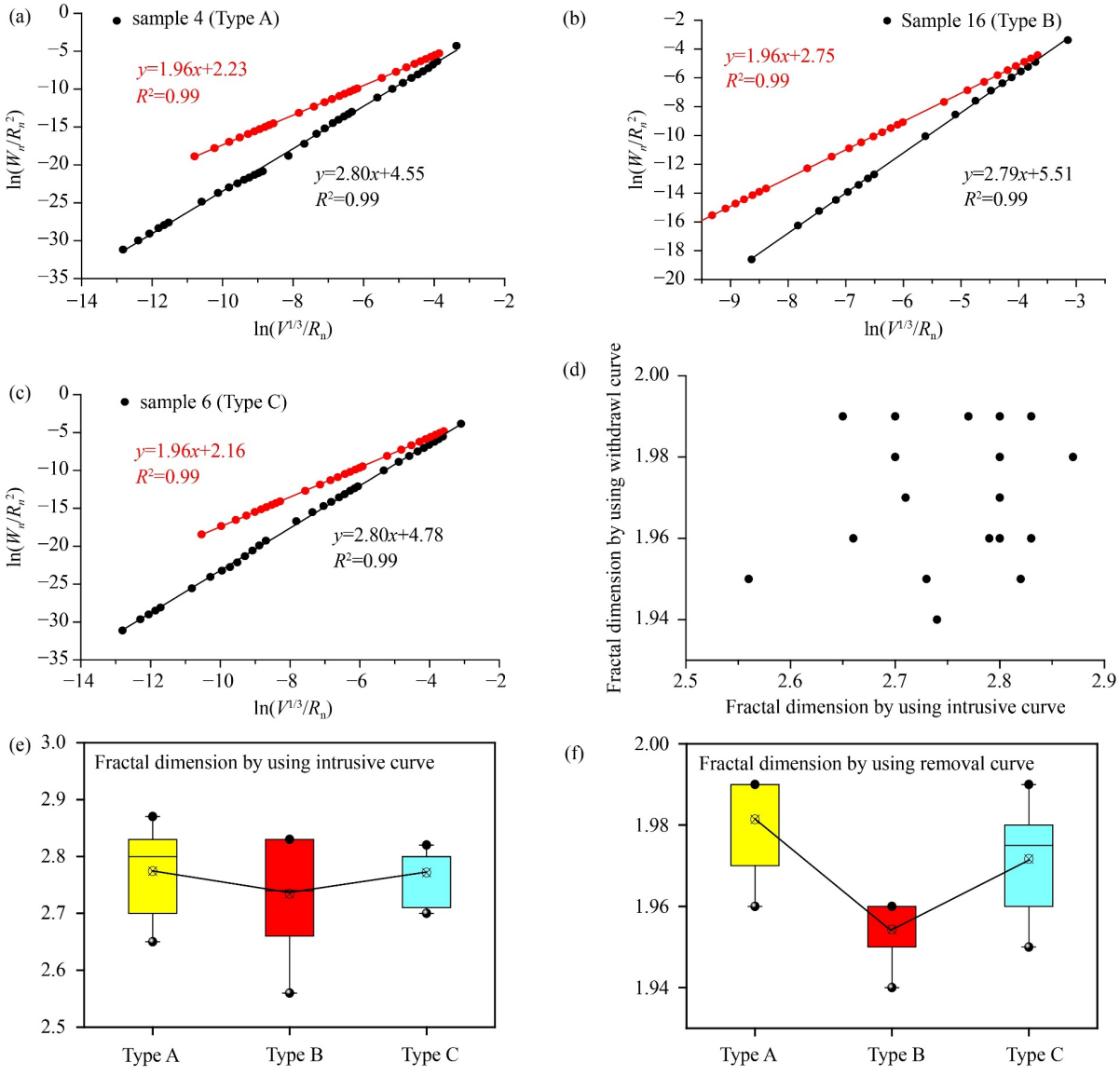

Fig. 5 Fractal characteristics of intrusion and removal curves using the thermodynamic model.

Figure 7(b) illustrates that the D_{-10}–D_0 and D_{-10}–D_{10} values obtained from the mercury withdrawal curves for type B samples are larger than those for type A and C samples, indicating that the fractal dimension obtained from the mercury withdrawal curves better reflects the differences among these samples.

3.4 Fractal characteristics using the Menger model

The results of the Menger model, based on Eq. (1) and the mercury injection and withdrawal curves, are shown in Fig. 8. The figure indicates that the mercury injection curve still exhibits fractal characteristics when using the multi-fractal model. However, the fractal characteristics of the mercury removal curve are similar to those of the mercury injection curve, indicating that the mercury removal curve, when analyzed using the Menger model, also displays fractal characteristics. It is important to note that the two fractal curves are nearly identical, indicating that the Menger model is not suitable to characterize the fractal characteristics of the mercury removal curves. Figure 9 shows that the fractal dimension obtained from the mercury injection curves is almost above 3, indicating a complex heterogeneity in the pore volume distribution in these samples.

4 Discussion

4.1 Relationship between pore structure parameters and mercury removal efficiency

Figure 10(a) shows that the mercury removal efficiency gradually increases with the increase in total pore volume. This can be attributed to the fact that samples with larger pore volumes exhibit mostly parallel plate-shaped pores,

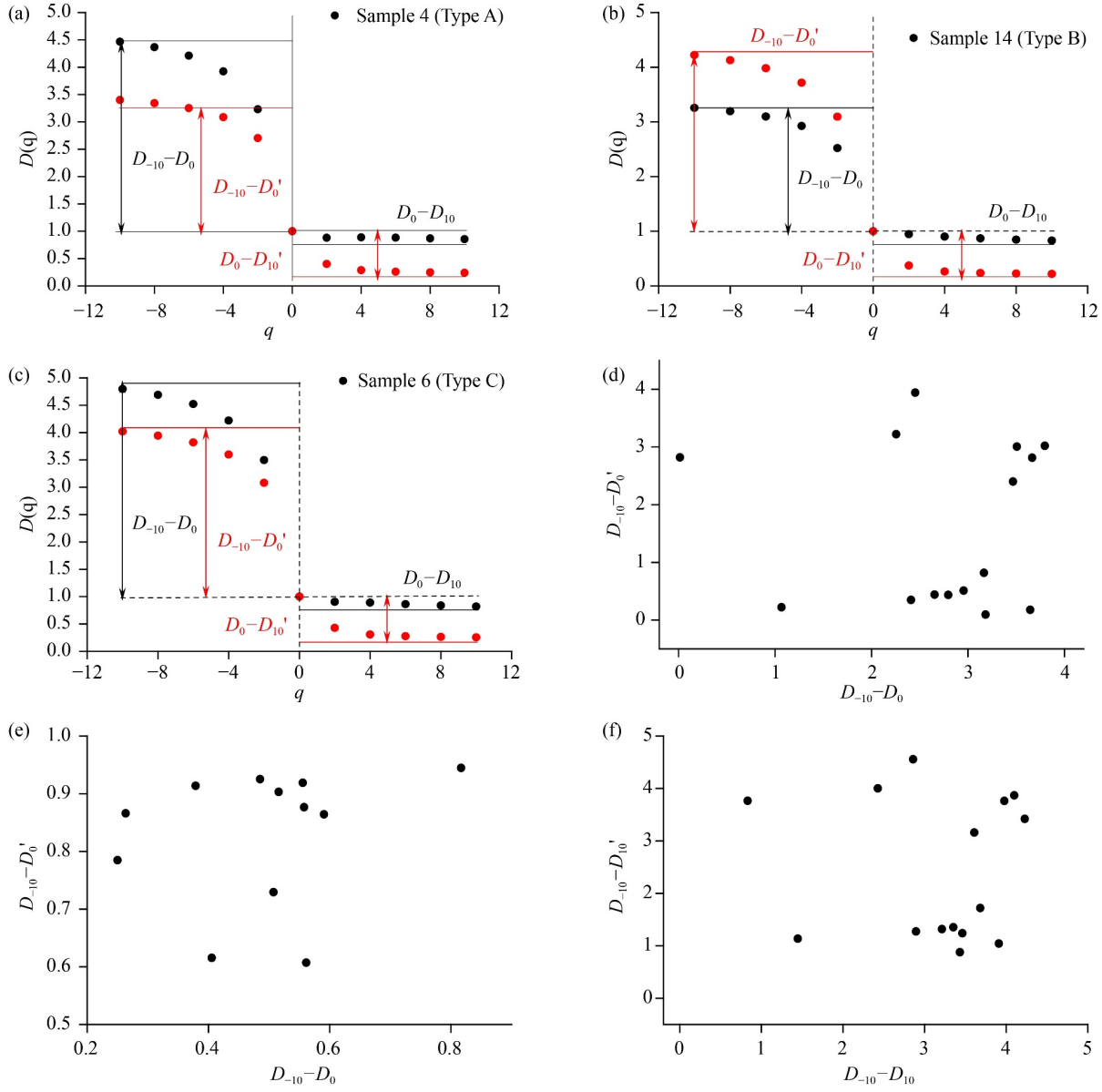

Fig. 6 Fractal characteristics of intrusion and withdrawal curves using the multi-fractal model.

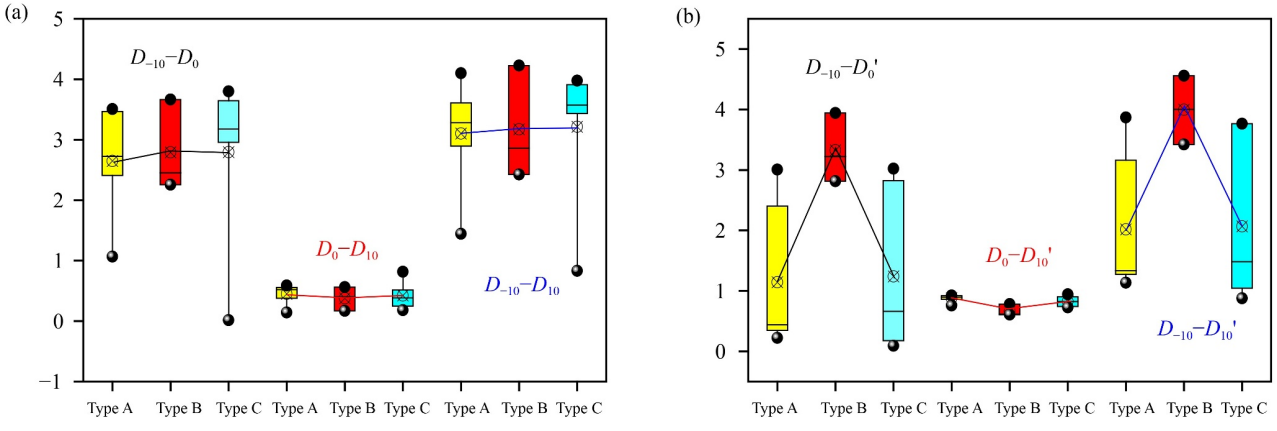

Fig. 7 Multifractal parameter variation of different sample types.

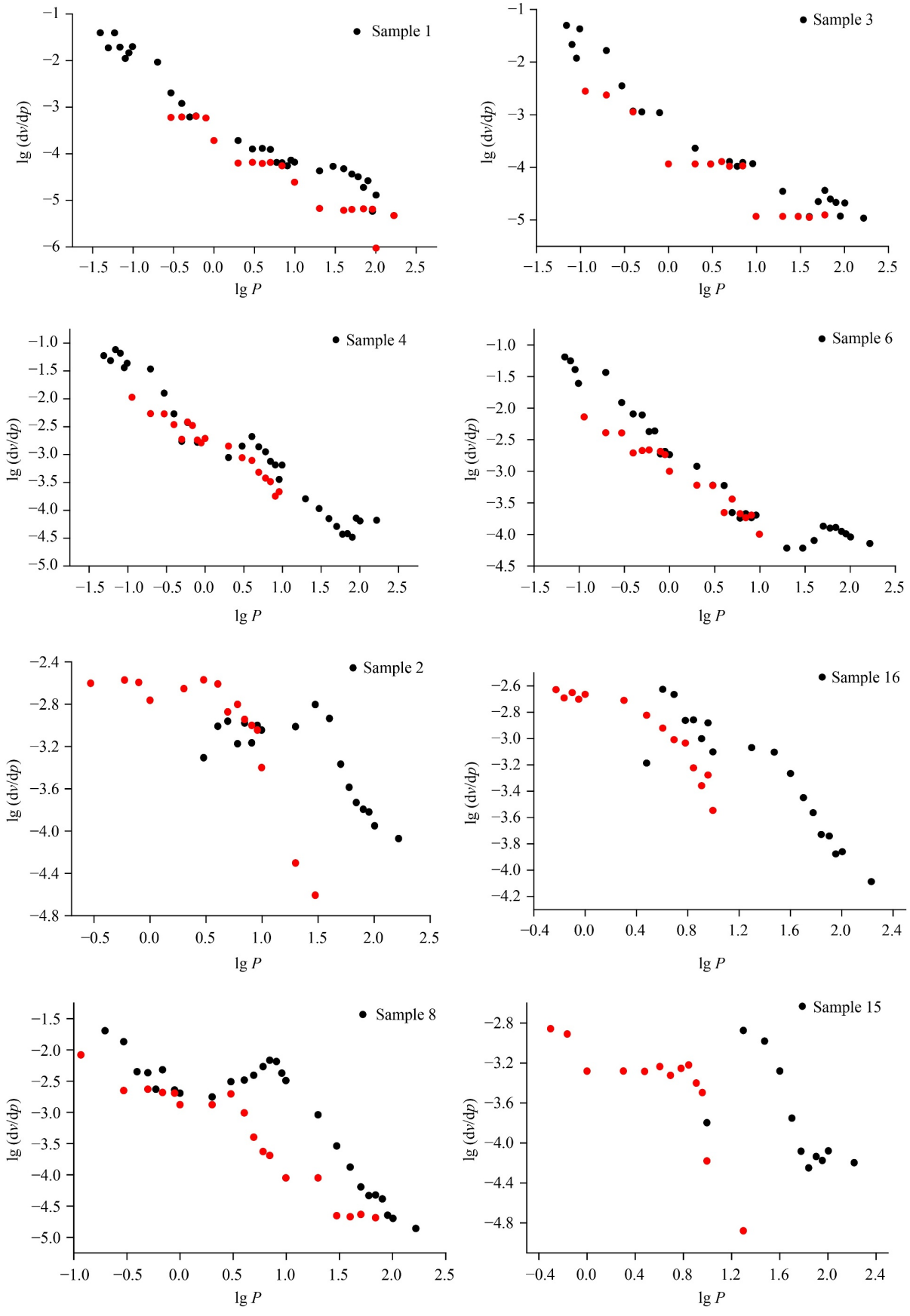

Fig. 8 Fractal curves of different sample types using the Menger model.

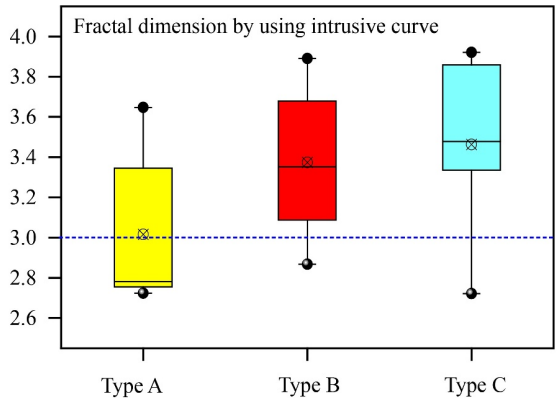

Fig. 9 Fractal dimension parameter variation using the Menger model of different sample types.

which promote good pore connectivity. Figures 10(b) and 10(c) reveal a certain correlation between the pore volume in the range of 100 to 1000 nm and the total pore volume, indicating that these pores play a significant role in determining the pore structure characteristics of all samples. Moreover, Fig. 10(d) shows that pores in the 100 to 1000 nm range restrict the mercury removal efficiency of samples, implying that these pores have control over the overall pore connectivity.

In contrast, Figs. 11(a) and 11(b) show no correlation between pore volume and mineral composition. However, there is a weak positive correlation between quartz content and mercury removal efficiency. This can be attributed to the fact that a higher quartz content facilitates the formation of micro-fractures and macro-pores, resulting in stronger connectivity (Figs. 11(c) and 11(d)).

4.2 Relationship between fractal dimension of intrusion/removal curves and related parameters

4.2.1 Thermodynamic model

Figure 12(a) shows that there is no obvious relationship between pore volume and fractal dimension when using mercury injection and removal curves. Figure 12(b) indicates a negative linear relationship between pore volume and fractal dimension when using the mercury removal curve, and there is no correlation between pore volume and fractal dimension when using the mercury injection curve. This suggests that the latter parameter better reflects mercury removal efficiency and pore connectivity. Figures 12(e) and 12(f) show that the fractal dimension, when using mercury removal curve, decreases as the pore volume in the range of 100−1000 nm and quartz content increase. However, there is no apparent relationship between pore structure parameters and fractal dimension when using the mercury injection curve, indicating that the fractal dimension derived from the

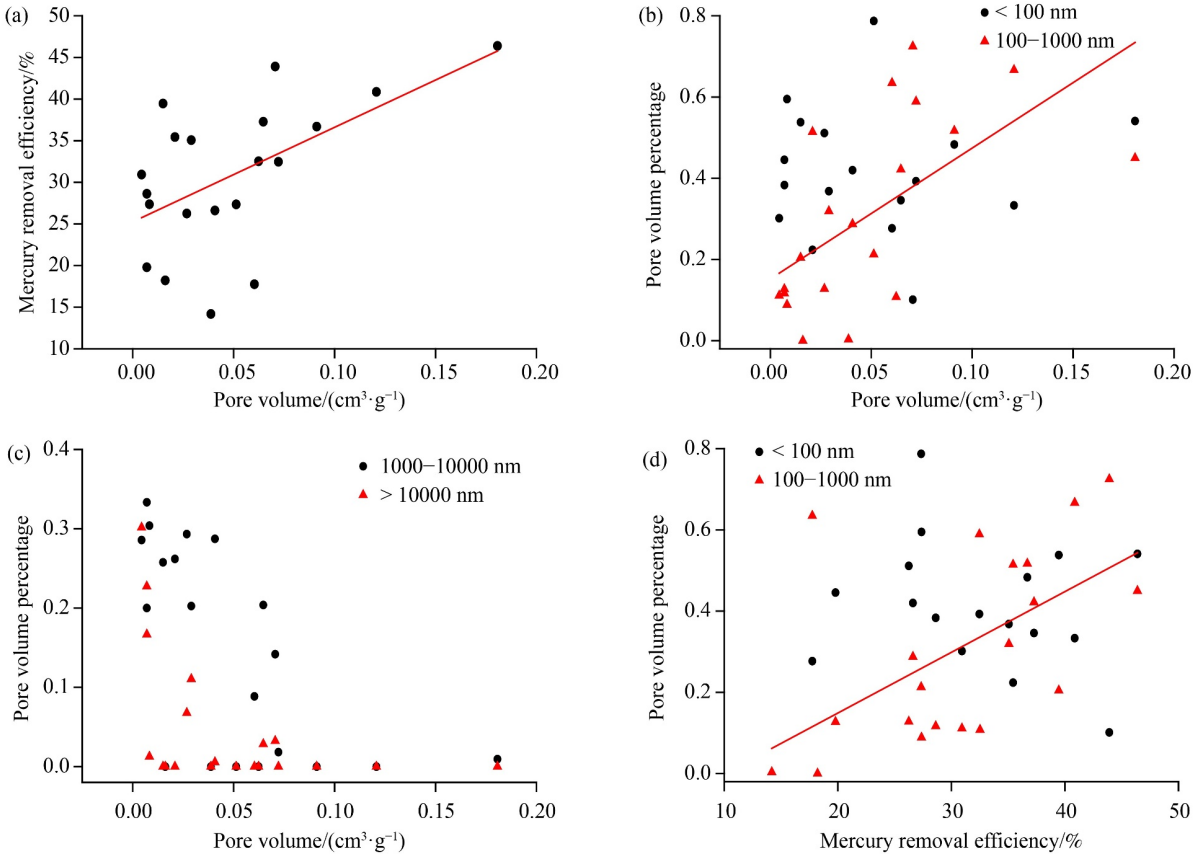

Fig. 10 Correlation analysis between pore structure parameters and mercury removal efficiency.

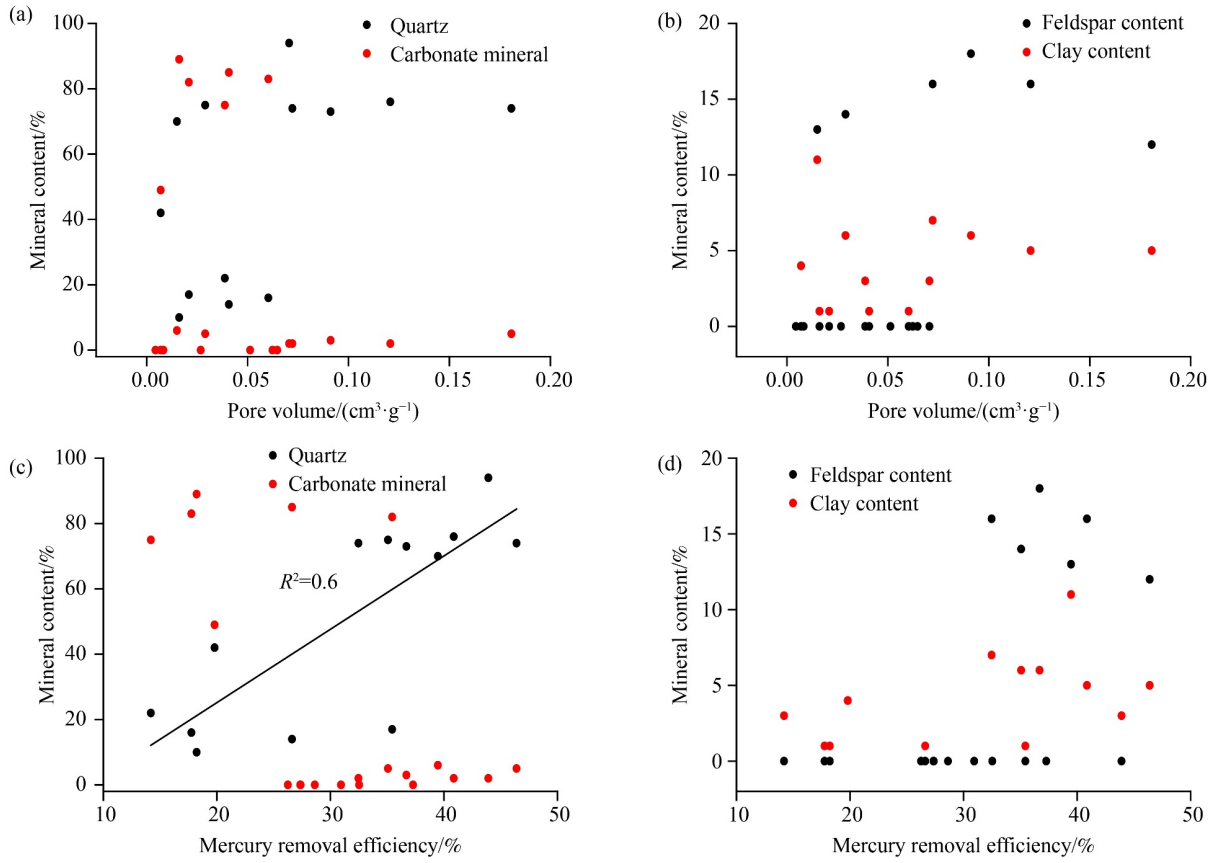

Fig. 11 Correlation analysis between pore structure parameters and mineral content.

mercury removal curve better reflects the heterogeneity of pore size distribution.

4.2.2 Multi-fractal model

Figure 13 shows a positive linear relationship between quartz content and D_{-10}–D_0 when using the mercury removal curve, whereas no correlation is observed between pore volume and fractal dimension when using the mercury injection curve. This indicates that latter parameter better reflects mercury removal efficiency and pore connectivity. Figure 13(b) shows a positive linear relationship between mercury removal efficiency and D_{-10}–D_0 when using the mercury injection curve, and no correlation is found between pore volume and fractal dimension when using the mercury removal curve.

In contrast, Figure 14 shows that D_0–D_{10} exhibits a strong linear relationship with pore structure parameters and mercury removal efficiency. As D_0–D_{10} increase, pore volume, mercury removal efficiency, and quartz content all decrease. Overall, multi-fractal parameters derived from the mercury removal curves better represent the heterogeneity of pore structure distribution.

4.3 Relationship between pore structure and fractal dimension using mercury removal curves

As mentioned above, both the thermodynamic and multifractal models can be used to characterize the fractal characteristics of mercury removal curves. Figure 15(a) shows that there is a good positive linear correlation between mercury removal efficiency and porosity, whereas its correlation with permeability is weak. Figures 15(b) and 15(c) show that the fractal dimension of the removal and injection curves, as determined by the thermodynamic model, has no clear correlation with porosity and permeability. This indicates that the applica bility of these two parameters in determining the porosity and permeability characteristics is limited. Furthermore, Figure 15(d) shows that the D_0–D_{10} parameter of the injection curve, calculated using the multi-fractal model, has no substantial correlation with porosity and permeability, indicating a weak applicability of this parameter in determining the characteristics of porosity and permeability. However, porosity and permeability exhibit a linear decrease with the increase of D_0–D_{10}' (withdrawal curve using the multi-fractal model), indicating that this parameter can be used to characterize the porosity-permeability structure of the reservoir (Fig. 15(e)). The difference in fractal dimension between the mercury injection and withdrawal curves shows a good linear positive correlation with porosity and permeability, indicating that D_0–D_{10}, as determined using the multi-fractal model, is a parameter suitable to characterize pore fracture structure.

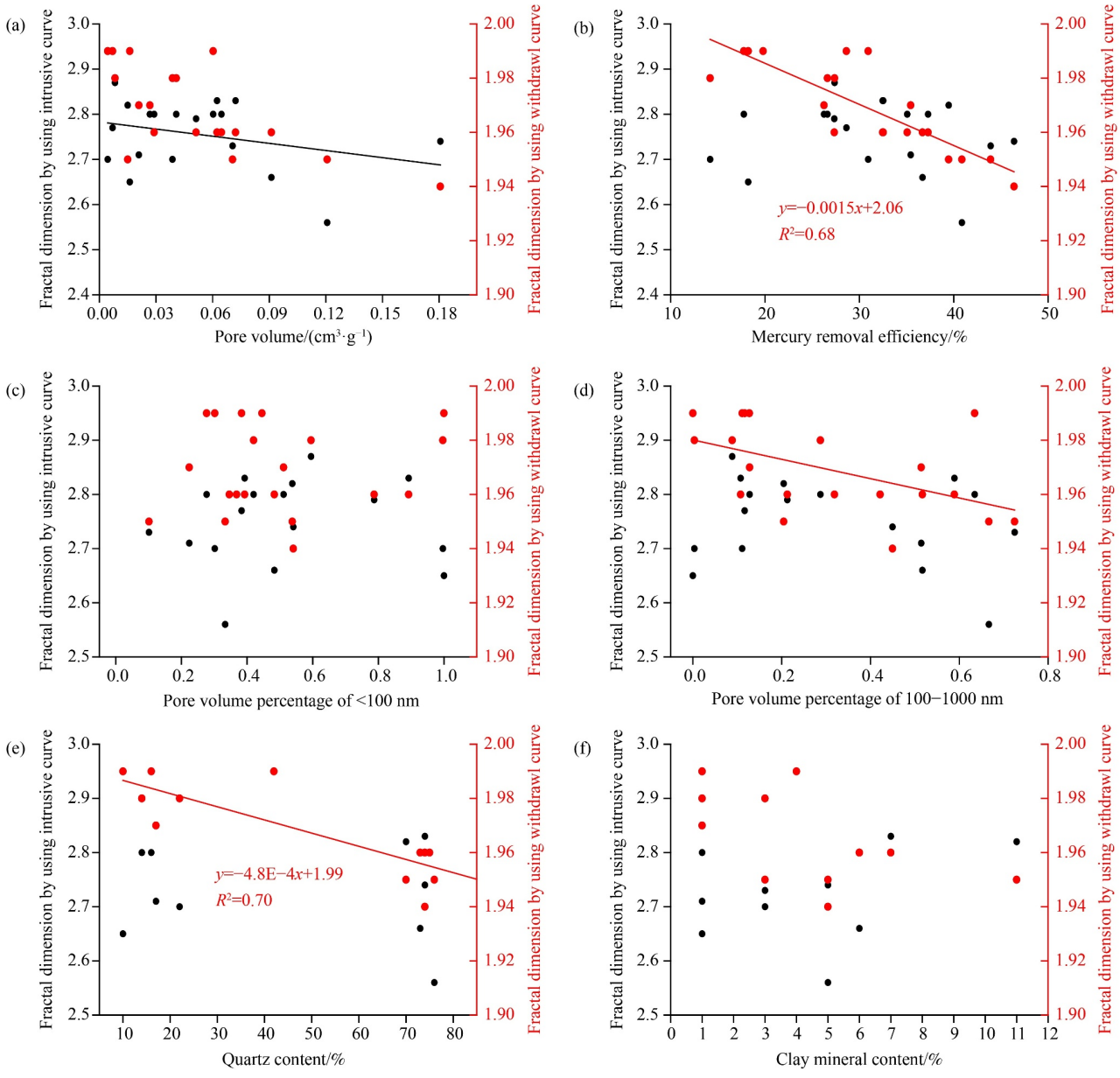

Fig. 12 Relationship between fractal dimension of intrusive/removal curves and related parameters (pore structure, mineral content).

5 Conclusions

1) The samples can be divided into three types based on mercury removal efficiency and total pore volume. Type A is characterized by lower total pore volume (< 0.08 $cm^3 \cdot g^{-1}$) and removal efficiency (< 30%), type B has lower total pore volume (< 0.08 $cm^3 \cdot g^{-1}$) and higher removal efficiency (> 30%), and type C is associated with larger total pore volume (> 0.08 $cm^3 \cdot g^{-1}$) and higher removal efficiency (> 30%).

2) Mercury removal efficiency shows no correlation with mineral composition and total pore volume, but it exhibits a clear positive linear correlation with the pore volume in the range of 100−1000 nm. In contrast to the Menger model, the mercury removal curve analyzed using the thermodynamics and multifractal models exhibits robust fractal characteristics. Compared with the mercury injection curve, the fractal dimension calculated based on the mercury withdrawal curve shows a good linear correlation with pore structure parameters and mineral components.

3) The difference in fractal dimension between the mercury injection and withdrawal curves demonstrate a good positive linear correlation with porosity and permeability, indicating that D_0–D_{10}, as determined using the multi-fractal model, is a parameter suitable for characterizing pore fracture structure. Further research should be conducted on fractal analysis using mercury removal curves.

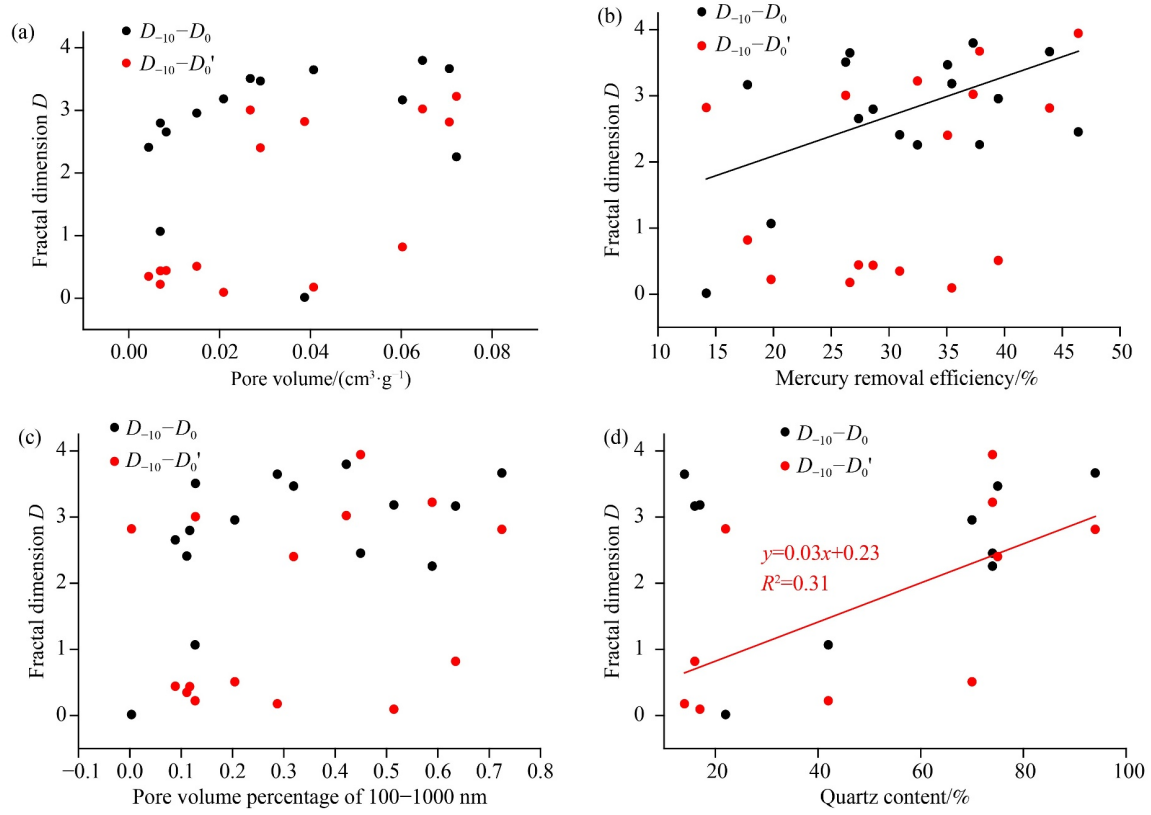

Fig. 13 Fractal characteristics of intrusive and removal curves by using a multi-fractal model.

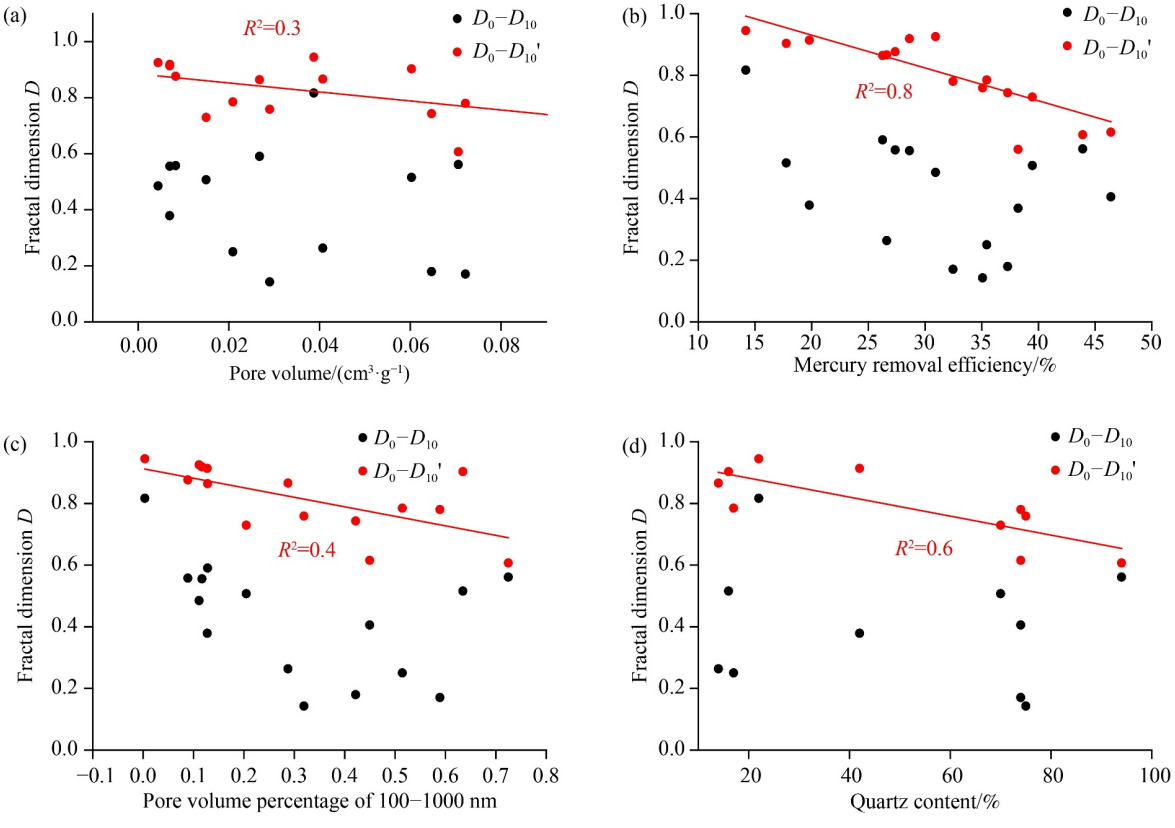

Fig. 14 Fractal characteristics of intrusion and removal curves using the multi-fractal model.

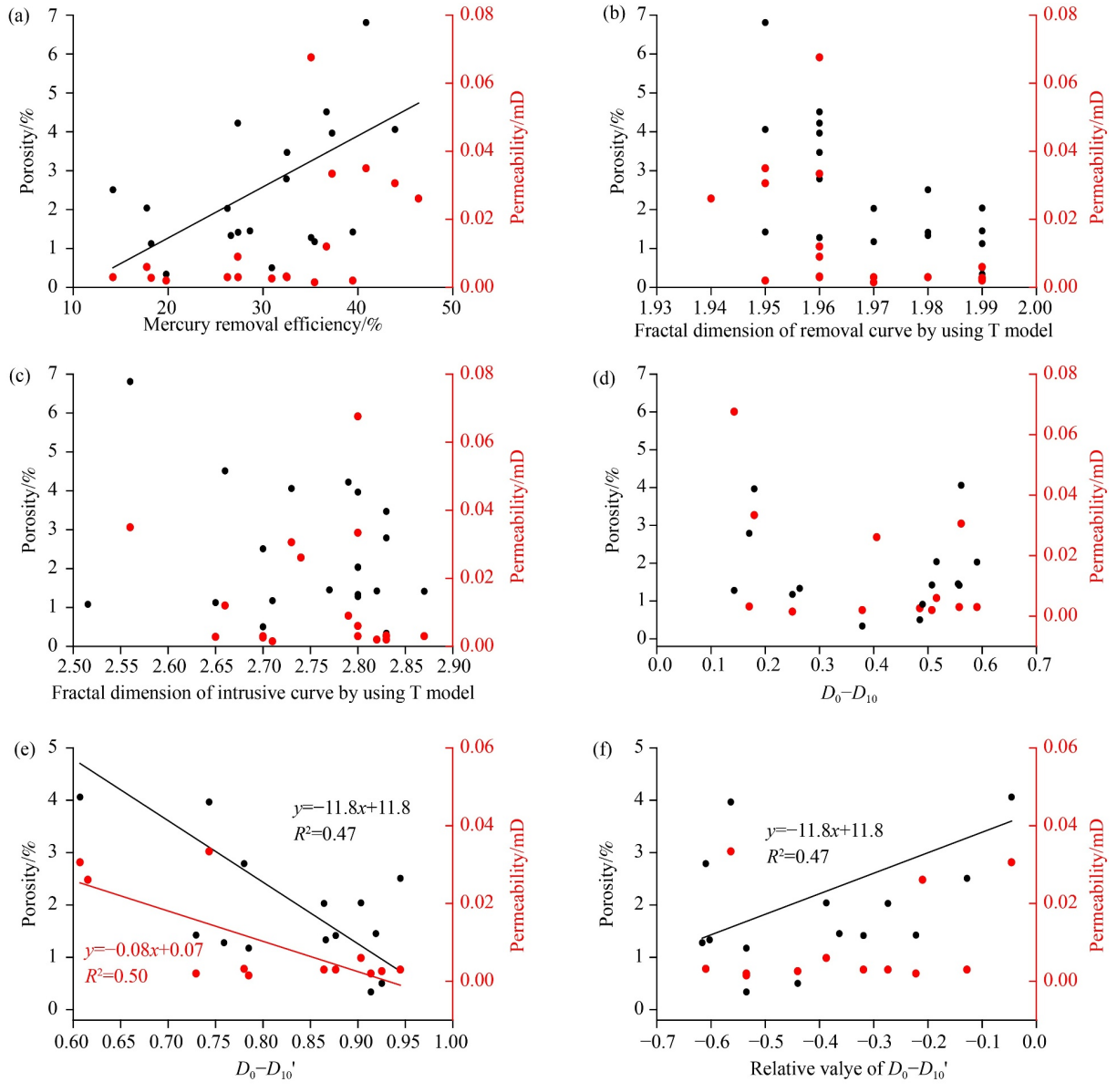

Fig. 15 Correlation analysis between pore structure parameters and fractal dimension.

Acknowledgments This research was sponsored by the Research Fund of Shandong Coalfield Geological Bureau (No. 2022-003).

Competing interests The authors declare that they have no competing interests.

References

Cai Y, Li Q, Liu D (2018). Insights into matrix compressibility of coals by mercury intrusion porosimetry and N_2 adsorption. Int J Coal Geol, 200: 199–212

Cai Y, Liu D, Pan Z (2016). Investigating the effects of seepage-pores and fractures on coal permeability by fractal analysis. Transp Porous Media, 111(2): 479–497

Guo X, Yao Y, Liu D (2014). Characteristics of coal matrix compressibility: an investigation by mercury intrusion porosimetry. Energy Fuels, 28(6): 3673–3678

He D F, Li D S, Zhang G W (2011). Formation and evolution of multi-cycle superposed Sichuan Basin, China. Chinese J Geo, 46(3): 589–606 (in Chinese)

Hou H H, Shao L Y, Tang Y, Li Y N, Liang G D, Xin Y L, Zhang J Q (2023). Coal seam correlation in terrestrial basins by sequence stratigraphy and its implications for palaeoclimate and palaeoenvironment evolution. J Earth Sci, 34(2): 1–15

Hou H H, Shao L Y, Tang Y, Zhao S, Yuan Y, Li Y N, Mu G Y, Zhou Y, Liang G D, Zhang J Q (2020). Quantitative characterization of low-rank coal reservoirs in the southern Junggar Basin, NW China: implications for pore structure evolution around the first coalification jump. Mar Pet Geol, 113: 104165

Hu Y, Guo Y, Shangguan J (2020). Fractal characteristics and model applicability for pores in tight gas sandstone reservoirs: a case study of the Upper Paleozoic in Ordos Basin. Energy Fuels, 34(12):

16059–16072

Knackstedt M A, Sahimi M, Roberts G W (1996). Fractal analysis of capillary pressure curves in reservoir rocks. Transport Porous Media, 24: 2–14

Lai J, Wang G, Wang Z (2018). A review on pore structure characterization in tight sandstones. Earth Sci Rev, 177: 436–457

Li Y, Yang J, Pan Z, Tong W (2020). Nanoscale pore structure and mechanical property analysis of coal: an insight combining AFM and SEM images. Fuel, 260: 116352

Peng C, Zou C, Yang Y, Zhang G, Wang W (2017). Fractal analysis of high rank coal from southeast Qinshui basin by using gas adsorption and mercury porosimetry. J Petrol Sci Eng, 156: 235–249

Schmitt M, Fernandes C P, Da Cunha Neto J A B, Wolf F G, Dos Santos V S S (2013). Characterization of pore systems in seal rocks using nitrogen gas adsorption combined with mercury injection capillary pressure techniques. Mar Pet Geol, 39(1): 138–149

Song Y, Jiang B, Li F L, Yan G Y, Yao Y P (2018). Applicability of fractal models and nano-pore's fractal characteristics for low middle rank tectonic deformed coals. Earth Sci, 43(5): 1611–1622 (in Chinese)

Su P H, Xia Z H, Qu L C, Yu W, Wang P, Li D W, Kong X W (2018). Fractal characteristics of low-permeability gas sandstones based on a new model for mercury intrusion porosimetry. J Nat Gas Sci Eng, 60: 246–255

Wang Z, Fu X, Pan J, Deng Z (2023). Effect of N_2/CO_2 injection and alternate injection on volume swelling/shrinkage strain of coal. Energy, 275: 127377

Zhang B, Liu W, Liu X (2006). Scale-dependent nature of the surface fractal dimension for bi- and multi-disperse porous solids by mercury porosimetry. Appl Surf Sci, (253): 1349–1355

Zhang F, Liu S W, Li Q G, Wang Z Q, Han Y G, Yang K, Wu F H (2009). LA-ICP-MS zircon U-Pb geochronology and geological significance of Xiba granitoids from Qinling, central China. Acta Scientiarum Naturalium Universitatis Pekinensisl, 45(5): 832–838 (in Chinese)

Zhang J J, Chu X X, Wei C T, Zhang P F, Zou M J, Wang M J, Quan F K, Ju W (2022a). Review on the application of low-field nuclear magnetic resonance technology in coalbed methane production simulation. ACS Omega, 7(30): 26298–26307

Zhang J J, Hu Q H, Chang X C, Qin Z Y, Zhang X Y, Marsh S, Grebby S, Agarwal V (2022b). Water saturation and distribution variation in coal reservoirs: intrusion and drainage experiments using one- and two-dimensional NMR techniques. Energy Fuels, 36(12): 6130–6143

Zhang J J, Qin Z Y, Han Y N, Wang H M, Hou M G, Yan G Y, Feng G J, Zhang X Y, Yin T T, Zhang H N, Wen S P (2022c). Pore-fracture distribution heterogeneity of shale reservoirs determined by using HPMI and LPN2 GA tests. Acta Geol Sin Eng Ed, 96(5): 1659–1672

Zhang P, Lu S, Li J, Chang X (2020). 1D and 2D nuclear magnetic resonance (NMR) relaxation behaviors of protons in clay, kerogen and oil-bearing shale rocks. Mar Pet Geol, 114: 104210

Zhao C J, Jiang Y L, Liu J D (2022). Occurrence and origin of chlorite and associated impact on tight sandstone reservoir quality: a case study of the Xujiahe Formation (NE Sichuan Basin, China). J Petrol Sci Eng, 209: 109859